Proceedings of ISERME 2025
19-20 September 2025
https://doi.org/10.31705/ISERME.2025.8

Mitigating Induced Seismicity Through Enhanced Fracture Stiffness in Fault Damage Zone

[*]Gang[1] MW, Sainoki[2] AS and Kodama[1] JI

[1]Graduate School of Engineering, Hokkaido University, Sapporo, Japan

[2]Faculty of Advanced Science and Technology, Kumamoto University, Kumamoto, Japan

[*]Corresponding author – gangmingwei_gmw@163.com

Abstract
In recent years, induced seismicity has increased, posing risks to underground facilities. Despite various mitigation efforts, their effectiveness remains limited due to the complex and heterogeneous stress states of natural geological structures. To address this challenge, this study proposes enhancing fracture stiffness in fault damage zones as a mitigation strategy. Using discrete element method (DEM) simulations, we show that increased stiffness can reduce seismic moments and radiate energy to around 40% of their original values, regardless of fracture orientation. The effect is stronger near the fault core, with higher fracture density and smaller fracture sizes, further amplifying the reduction. These findings offer a conceptual basis for mitigating seismic hazards through targeted modification of fracture properties.

Keywords: DEM, Fracture stiffness, Induced seismicity, Seismic hazards mitigation

1 Introduction

Induced seismicity has become increasingly widespread, raising significant concerns. Driven by the rising demand for mineral and energy resource extraction, mining-induced seismicity has been studied for decades and continues to draw public attention due to the associated seismic risks. Although mining-induced seismicity releases less energy compared to natural earthquakes, they occur more frequently and typically at shallow depths, within a few kilometres.

Mining-induced seismicity has been documented globally [1-2], for almost all underground mines and different rock types. Many approaches [3-4] have been employed to mitigate seismic risks in underground mining. For example, hydraulic fracturing technology, deep-hole blasting and monitoring technique. However, due to the limited underground space and complex geological conditions in underground mines, these methods are often insufficient for mitigating the scale of mining-induced seismicity. Hence, it is necessary to develop a more effective method to reduce the associated damage.

According to the slip-weaking model **Error! R eference source not found.**, it can be concluded that an increase in the stiffness of the surrounding rock mass leads to a reduction in radiated energy. This provides a new perspective for mitigating seismic energy associated with induced seismicity.

In this study, the heterogeneous mechanical behaviour and stress state of the fault damage zone are reproduced using a DEM model with densely fractured networks. Then, the effect of enhanced fracture stiffness is investigated by increasing the normal and shear stiffnesses of the fractures in the damage zone.

2 Simulation method

2.1 Model construction

A model with a size of 10 m×10 m×10 m is constructed and the fault core is simulated as a discontinuous plane with a specific joint at the center of the model (Figure 1). Disk-shaped fractures in a fault damage zone are generated following the power low function, which suggests that the density of fractures decreases exponentially with increasing distance from the fault (Figure 2). The generation of discrete fracture network within the fault damage zone requires the specification of key parameters, including fracture density, length, and orientation. Fracture density can be employed with the following power law function **Error! Reference source not found.**:

$$P_{10} = \alpha d^{\beta} \tag{1}$$

where the coefficient α corresponds to the maximum fracture density adjacent to the fault core; β serves as a scaling factor; and d represents the distance from the fault core. Regarding fracture length, a cumulative density function is employed **Error! Reference source not found.**.

$$F(l) = \frac{l_{min}^{1-a} - l^{1-a}}{l_{min}^{1-a} - l_{max}^{1-a}} \tag{2}$$

where a determines the ratio of small to large fractures in the network; l_{max} and l_{min} define the maximum and minimum fracture lengths, respectively. Finally, the orientation of fractures is defined using the Fisher function, as described by the following equation **Error! Reference source not found.**.

$$f(\theta) = \frac{k \sin\theta e^{\cos\theta}}{e^{k} - e^{-k}} \tag{3}$$

where k and θ denote the Fisher constant and the angular deviation from the mean vector, respectively. The parameters employed in Eqs. (1) to (3) are as follows: α = 30, β = 0.8, l_{min} = 2 m, l_{max} = 10 m, a = 2.5 and k = 40.

The host rock within the fault damage zone is assumed to be granite. The Young's modulus of the intact rock is set to 60 GPa, with the Poisson's ratio of 0.2, which falls within the typical range of 0.17 to 0.30. A density of 2600 kg/m^3 is also applied to the model. The initial normal and shear stiffnesses of the fractures, denoted as K_{n} and K_{s}, are set to 30 GPa/m and 10 GPa/m, respectively. In this study, K_{n} and K_{s} are increased by 5 times to verify the effect of enhanced stiffness on seismic source parameters.

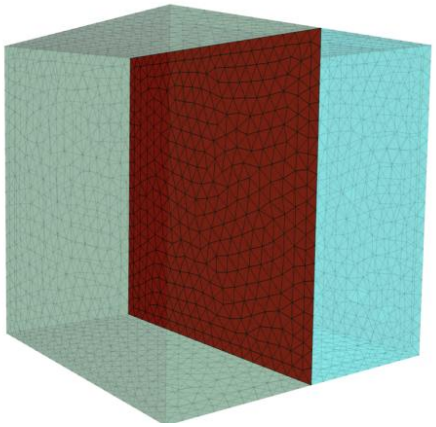

Figure 1: Numerical model

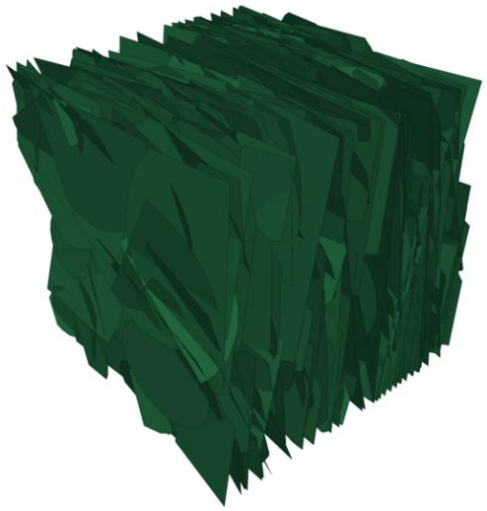

Figure 2: Fracture network in a fault damage zone

2.2 Simulation of seismic events

As the first step, an initial stress state is simulated by applying regional stresses to the model external boundaries. It is to be noted that the direction of gravity is rotated at 20° in anticlockwise direction to simulate a fault dipping at 70°. The reason why such a vertical fault is simulated in Fig. 1 is that a complicated procedure needs to be taken to generate a discrete fracture network (DFN) for dipping faults. The stress applied to the model boundary correspond to those at a depth of 2000 m. As for the bottom boundary, the displacement in all directions is fixed at the four vertices to prevent the rigid body movement. Except for the four vertices, the displacement on the bottom boundary is constrained only in the z-direction.
After simulating the initial stress state, the effective normal stress on the fault plane is gradually decreased in a stepwise manner in the circular region on the fault as shown in Figure

3The radius of this circular region is 1.5 m. In each analysis stage, the effective normal stress is decreased by 2.0 MPa. Cumulatively, 20 MPa of the effective normal stress is decreased (Figure 4). This method assumes that on-fault induced seismicity is caused by unclamping of faults, i.e., the effective normal stress reduction due to rock mass excavation, fluid injection, etc.

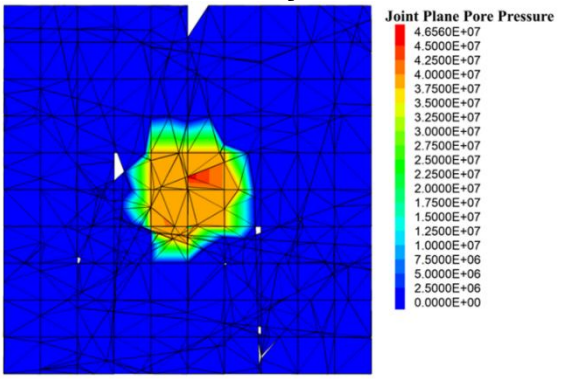

Figure 3: Stress reduction region

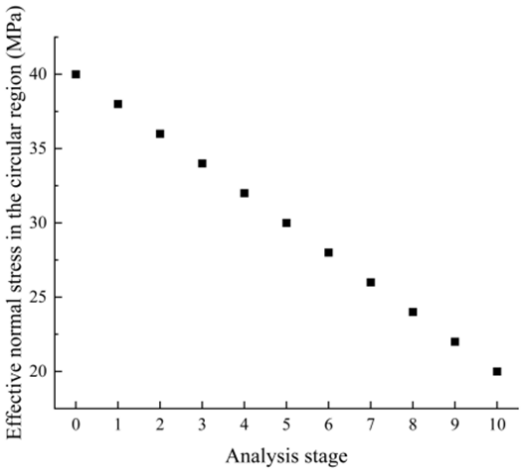

Figure 4: Stress reduction stage

3 Results

Seismic source parameters, such as seismically radiated energy and seismic moment, serve as key indicators for assessing seismic damage. A decline in these parameters indicates a potential mitigation of seismic hazards. In this study, the seismic moment is defined by the following equation **Error! Reference source not found.**:

$$M_0 = \mu DS \tag{4}$$

where μ is the shear modulus of the surrounding rock, D is the average shear displacement on the fault, and S is the fault area that slipped. The seismically radiated energy can be estimated by integrating the energy flux over time and space during rupture propagation **Error! Reference s ource not found.**:

$$E_R = \left(\int \rho\beta \int \dot{u}^2 \, dt \right) dS \tag{5}$$

where ρ and β represent the density of the surrounding rock mass and shear wave velocity, respectively; t and $\dot{u}$ are time and slip rate, respectively.

Figure 5 shows the seismic results for different depths. As shown, the seismic moment and seismically radiated energy are decreased to around 40% of their original values when the stiffnesses are increased by 5 times. At the same time, the seismic moment and seismically radiated energy are decreased to 38% of their original values when the stiffnesses are increased by 5 times. There is almost no difference between these two situations, indicating that the impact of mining depth on seismic source parameters is minimal.

Figure 6 illustrates the seismic results for various fracture densities. As can be seen, the seismic moment and seismically radiated energy are reduced to 40% of their original values when the stiffnesses are increased by 5 times. However, when the fracture density decreases, these two parameters only decrease to 80% of their original values. This suggests that the effectiveness of enhanced stiffness depends on the number of fractures and network characteristics. In the case of high fracture density, the total fracture surface area increases significantly, providing a wider interface for energy dissipation. In addition, the increase in density promotes stronger connectivity between adjacent fractures, effectively forming more continuous and interacting damage zones, making it more sensitive to changes in the fracture stiffness.

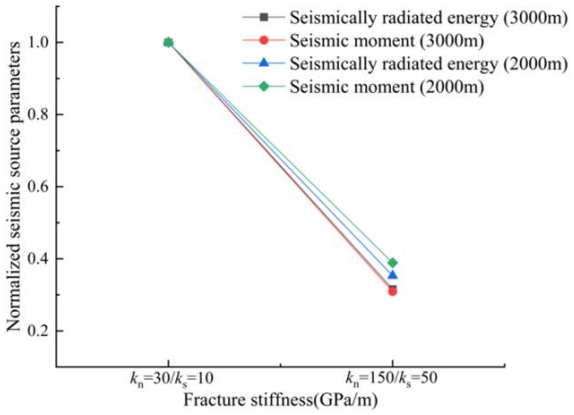

Figure 5: Seismic results for each depth

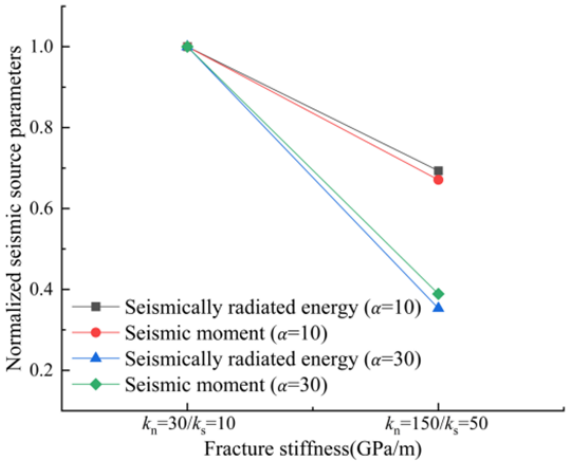

Figure 6: Seismic results for each fracture density

4 Conclusion and discussion

3DEC (Three-Dimensional Distinct Element Code) is applied in this study to build a cubic model with a side length of 10 m and a DFN is constructed based on power law function. A fault core is simulated with a specific joint at the centre of the model. Using the DEM model, a complex, heterogeneous stress state with stress anomalies is simulated by applying stresses on the model outer boundaries. Seismicity is induced by decreasing the effective normal stress on the fault plane by 2.0 MPa in each analysis stage. The results indicate that the depth of excavation does not affect the effect of enhanced stiffness on seismic source parameters, but the fracture density varies. The higher the fracture density in the damage zone, the more significant the impact of enhanced stiffness on seismic source parameters.

References

[1] Grigoli. F and Cesca. S,"Current challenges in monitoring, discrimination, and management of induced seismicity related to underground industrial activities: A European perspective", Rev *Geophys*. 55 (2), 2017.

[2] Foulger. GR, "Global review of human-induced earthquakes", *Earth-Sci. Rev*, 178, 2018.

[3] Shen. WL and Yu. Y, "Response and control technology for entry loaded by mining abutment stress of a thick hard roof", *Int. J. Rock Mech. Min. Sci*, 90, 26-34, 2018.

[4] Wang. F and Tu. H, "Deep-hole pre-split blasting mechanism and its application for controlled roof caving in shallow depth seams", *Int. J. Rock Mech. Min. Sci*, 64, 112-121, 2013.

[5] Venkataraman. A and Kanamori. H, "Observational constraints on the fracture energy of subduction zone earthquakes", *J. Geophys. Res.: Solid Earth,* 109(B5), 2004.

[6] Agosta. F and Alessandroni. M, "From fractures to flow: A field-based quantitative analysis of an outcropping carbonate reservoir", *Tectonophysics*, 490 (3-4), 197-213, 2010.

[7] Gutierrez. M and Youn. DJ, "Effects of fracture distribution and length scale on the equivalent continuum elastic compliance of fractured rock masses", *J. Rock Mech. Geotech. Eng,* 7 (6), 626-637, 2015.

[8] Bandis. SC and Lumsden. AC., "Fundamentals of rock joint deformation", *In International Journal of Rock Mechanics and Mining Sciences & Geomechanics Abstracts*, 20 (6), 249-268, 1983.

[9] Kanamori. H and Rivera. L, "Energy partitioning during an earthquake", *Geophys. Monogr. Ser*, 170, 3-13, 2006.

[10] McGarr. A and Fletcher. JB, "Mapping apparent stress and energy radiation over fault zones of major earthquakes", *Bull. Seismol. Soc. Am*, 92 (5), 1633-1646, 2002.